City Research Online

City, University of London Institutional Repository

Influence of Fluid Temperature Gradient on the Flow within the Shaft Gap of a PLR Pump

W. Qian

University of Michigan-Shanghai Jiao Tong University Joint Institute, Shanghai Jiao Tong University, Shanghai, China
399300@163.com

B. Rosic

Osney Thermo-Fluids Laboratory, Department of Engineering Science. University of Oxford, Oxford, UK
budimir.rosic@eng.ox.ac.uk

Q. Zhang

Department of Mechanical and Aeronautical Engineering
School of Engineering and Mathematical Sciences
City University London, UK
Qiang.Zhang@city.ac.uk

B. Khanal

Cranfield University, Shrivenham, SN6 8LA, UK
b.khanal@cranfield.ac.uk

ABSTRACT

In nuclear power plants the Primary-Loop Recirculation (PLR) pump circulates the high temperature/high-pressure coolant in order to remove the thermal energy generated within the reactor. The pump is sealed using the cold purge flow in the shaft seal gap between the rotating shaft and stationary casing, where different forms of Taylor-Couette flow instabilities develop. Due to the temperature difference between the hot recirculating water and the cold purge water (of order of two hundred degrees Celsius), the flow instabilities in the gap cause temperature fluctuations, which can lead to shaft or casing thermal fatigue cracks. The present work numerically investigated the influence of temperature difference and rotating speed on the structure and dynamics of the Taylor- Couette flow instabilities. The CFD solver used in this study was extensively validated against the experimental data published in the open literature. Influence of temperature difference on the fluid dynamics of Taylor vortices was investigated in this study. With large temperature difference, the structure of the Taylor vortices is greatly stretched at the interface region between the annulus gap and the lower recirculating cavity. Higher temperature difference and rotating speed induce lower fluctuating frequency and smaller circumferential wave number of Taylor vortices. However, the azimuthal wave speed remains unchanged with all the cases tested. The predicted axial location of the maximum temperature fluctuation on the shaft is in a good agreement with the experimental data, identifying the region potentially affected by the thermal fatigue. The physical understandings of such flow instabilities presented in this paper would be useful for future PLR pump design optimization.

INTRODUCTION

Taylor-Couette Flow Phenomena

Different forms of Taylor-Couette flow instabilities that can develop within the narrow gap of two concentric rotating cylinders, have been extensively investigated by many researchers. At low Reynolds numbers (Re) the laminar Couette flow regime is established [1]. As the rotational speed of cylinders increases a family of different flow instabilities, Taylor-Couette flows is developed [2].

Andereck et al. [3] presented a detailed map showing different types of Taylor vortices that can form under different rotating speed of cylinders. The critical angular velocity (or Taylor number) for the onset of Taylor vortices is strongly dependent upon the cylindrical gap radius ratio (η). By applying linear stability theory, Sparow et al. [4] and Roberts [5] showed that the critical Taylor number would increase with smaller radius ratio (wider gap). The experimental work of Cognet [6] also confirmed these trend. Burkhalter and Koschmieder [7] found that the perturbation caused by the imperfection in their experiment did not have any effect on the stability of the toroidal vortices as long as Taylor vortices were present.

With the further increase in rotational speed, wavy Taylor-Couette flow is established, characterized by wavy vortices azimuthally travelling around the annular gap and fluctuating along the axis direction. The rotational speed for forming wavy Taylor vortices is approximately 20 percent higher than the critical value for onset of Taylor vortices. Kingt [8] reported that the wave speed is strongly linked to the radius ratio of the two cylinders, and is not significantly affected by Taylor number. With even higher rotational speed, wavy Taylor–Couette flow becomes chaotic and finally becomes fully turbulent.

Adding axial flow to the Taylor-Couette flows results in formation of another flow family – Taylore-Couette-Poiseuille flows. These flow stabilities caused by superposition of rotational and axial flows were experimentally demonstrated by Wereley and Lueptow [9]. The experimental investigation by Becker and Kaye [10] showed that addition of axial flow delays the transition process that leads to formation of Taylor vortices. The study of Martin and Hasoon [11] indicates the same gap radius ratio η effect on critical Taylor number as in the cases without axial flow.

Fig. 1. Schematic of a PLR pump detail [12], and enlarged view of the flow between the pump shaft and casing.

PLR Pump Application

In boiling water nuclear reactor power plants, the Primary-Loop Recirculation (PLR) pump circulates the high temperature/high pressure coolant in order to remove the thermal energy generated within the reactor. The pump is sealed using the cold purge flow in the shaft-casing gap where the Taylor flow instabilities develop. Due to the temperature

difference between the hot recirculating water and the cold purge water (in the order of two hundred degrees Celsius), the temperature fluctuations could potentially lead to shaft or casing thermal fatigue cracks. Figure 1 shows a schematic of a PLR pump shaft detail given by Narabayashi et al. [12]. The purge coolant water enters the gap from the top of the shaft and eventually mixes with the hot water in the casing impeller cavity. This important engineering problem was originally experimentally investigated by Narabayashi et al. [12] and Kato et al. [13]. They reported that the temperature fluctuations (and eventually thermal fatigue) in the shaft-casing gap were caused by the wavy Taylor vortices which periodically bring the hot and cold water close to the rotor shaft and casing cover. The axial temperature difference in their study was $60℃$, while the temperature difference in real operating conditions could be as high as $250℃$. Watanabe et al. [14] observed that the amplitude of temperature fluctuations would increase with larger purge water flow rate. Their study proposed a seal purge heater concept to mitigate the amplitude of temperature fluctuations by heating the cold water before it entered the annulus gap and downstream cavity. Due to the experimental difficulties associated with the extremely high radius ratio (0.993), these experimental studies only provided some general observation of the temperature fluctuation. No detailed flow physics were revealed.

There are several studies which looked into the heat transfer phenomena associated with the Taylor-Couette flow [10, 15-17]. Most of these investigations focused on measurements of the inner cylinder heat transfer coefficients for cases with radial temperature gradient within the annulus gap. A series of correlation formulas for average Nusselt number calculation along the whole cylindrical axis were reported by Fenot et al. [18]. Recently, Liu et al. [19] showed that the wavy frequency of the vortices would be lower when temperature of the flow is increased, and there is an accelerating effect on their

formation when the inner cylinder is much cooler than that of the outer one. Effect of temperature gradient brought by the axial cold purge flow has not been investigated in the studies listed above.

Objectives and Outline of the Presented Work

The present numerical study aims to understand how the large temperature differences between cold purge flow and hot recirculating water affect the flow dynamics at shaft-casing gap of a PLR pump.

In the first part of the paper, three different experimental test cases, available in open literature, that focus on different aspects of Taylor instabilities, were modelled in order to test the capabilities of the flow solver used in this study.

- Test Case 1: Wavelength analysis (Burkhalter and Koschmieder [7])

- Test Case 2: Wavy Taylor-Couette Flow (Kingt [8])

- Test Case 3 :Heat transfer in Taylor-Couette Flow (Ball et al. [20])

In the second part of the paper, a simplified, but representative geometry of the interface between the shaft-casing gap and the pump cavity was modelled. The investigation starts by analysing the flowfield in the shaft-casing gap for the case with no temperature difference between the purge flow and the main pump flow. The temperature difference of 243 K between two fluids was then introduced, followed by a detailed analysis of the unsteady flow and temperature field. In the final study presented in this paper, the temperature difference between two flows was varied in order to estimate the vertical penetration depth of the hot fluid inside the gap, an important parameter for the pump design.

The results obtained in this paper could potentially help the development of an effective control solution to mitigate thermal fatigue in different components caused by flow instabilities in the shaft gap.

COMPUTATIONAL DETAILS

The commercial CFD solver ANSYS FLUENT was used to simulate all the cases considered in this paper. FLUENT is a finite-volume solver and is capable of simulating both steady and unsteady flow problems with a wide range of fluid properties. Fully compressible 3D viscous simulations based on the PLR pump shaft operating boundary conditions were performed in the present study. Since large variations of viscosity, density, and thermal conductivity of the water exist within the temperature ranges being investigated in this paper, density-based solver in FLUENT (fully compressible flow solver option) was chosen for all the CFD simulations.

The spatial discretization used was flux difference splitting based on the second-order upwind (default option for compressible flow in FLUENT) and a second-order implicit scheme adapted for temporal discretization. A solver was chosen to ensure a fully compressible solution and a constant time step of at least 1/50 over one fundamental period was maintained for the unsteady simulation (constant time-stepping is essential for the time consistency of the resolved unsteady structures). As an example, the wavy frequency was generally observed at around the cylinder rotating frequency. Therefore, for the case with a rotational speed of 127 rad/s, the time required for one complete rotation will be 0.0495 sec. To ensure that transient phenomena were accurately resolved, each period was computed using 50 discrete time steps, which results in a time step size of 0.001 sec. Initially, the simulations were run for a total of 15000 time steps to achieve fully

resolved unsteady solutions. Then the unsteady monitors were activated and the flow simulations were run for 1000 more time steps to record the corresponding unsteady information. For further unsteady flow analysis, Fast Fourier Transforms (FFT) method was applied and all the FFT data presented in this paper correspond to the spectral analysis of the unsteady signals for the 1000 time steps.

Mesh independence study was performed by varying grid numbers along the axial, radial and circumferential directions. It was established that a computational domain with $100 \times 60 \times 400$ grid points (along the circumferential, radial, and axial directions) was enough to provide mesh independent results. This was verified by monitoring the Taylor vortices number along the axial direction and the shape of vortical structure. This computational grid topology was maintained for all the CFD simulations performed in this paper.

VALIDATION TEST CASES

This section assesses the suitability of the CFD method and the solver employed to simulate the flow phenomena in the present study. The first validation case compares the simulated axial wavelengths with the experimental data, in which the flow regime is within the first stage of the Taylor vortices formation. The second validation case verifies the solver's capability of predicting the flow properties when it is within the second stage of Taylor-Couette flow. Finally, a third case was used to validate the thermal prediction capability of the solver. In the first and the second cases, the working fluid was water whereas the working fluid in the third case was air.

Test Case 1: Wavelength Analysis [7]

As the first validation case, conditions in the work of Burkhalter and Koschmieder [7] were simulated. They studied the axial wavelength of Taylor vortices at varying Taylor

numbers under a sudden start situation, which meant that the time taken by the inner

cylinder to accelerate to the preset rotating speed was much smaller than the fluid

dissipation time. This was also the reason why the present work chose this study as a

reference, since the setting flow variables at the boundary of a rotating wall to constant

values has the same effect as with a sudden start in real scenario. They provided detailed

boundary conditions and a full set of results regarding Taylor number and wavelength

relations. The geometry applied in the present validation work was a simple hollow cylinder

and its dimensions were matched with those in the real experiment: the height of the

cylinder was 0.9144 m, the inner and outer radii were 0.04572 m and 0.06285 m

respectively (η=0.727). Here the Taylor number was defined as,

$$Ta = \frac{2\eta^2}{1-\eta^2} \frac{(\Omega d^2)^2}{\nu^2}, \tag{1}$$

where Ω is the angular velocity, d is the gap width, and ν is the kinematic viscosity. Ta_c

(equal to 69.2 based on the simulation) is the critical Taylor number, which is the minimum

value at which Taylor vortices may appear. The axial wavelength (λ) of Taylor vortices was

defined as,

$$\lambda = \frac{L-E}{Nd}, \tag{2}$$

where L is the height of the cylinder, E is the summation of the size of the two end vortices,

N is the number of the vortex rings (half of the total vortices except for the end ones).
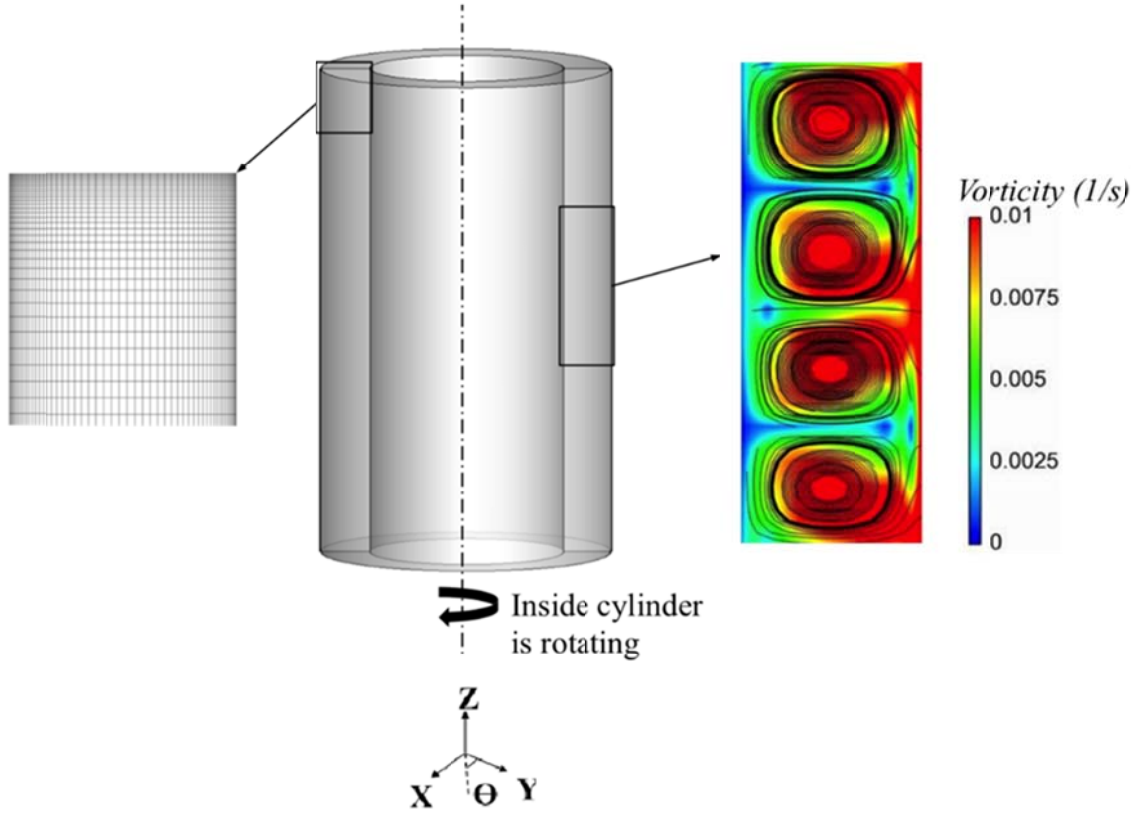
Fig. 2. Computational domain and an instantaneous vorticity contours for a validation test

case. (Ta=83.74 η=0.727)

As discussed in the paper by Burkhalter and Koschmieder [7], the viscosity of the fluid has little effect on the wavelength. They also concluded that the ends of the annulus gap (whether free surface or wall) had no significant influence on their experiment results. Therefore, for all the validation cases presented here, the end walls were set to be rotating at the same speed as the inner cylinder. With all the other boundary conditions fixed, several numerical simulations were run over a range of Taylor numbers. Water was selected as the working fluid in all the cases investigated in this paper, and the default water property values were employed. The resulting structure of the Taylor vortices in the computed result is shown in Fig.2 illustrated by the local instantaneous vorticity contours and streamlines. Figure 3 shows the comparison of the computed wavelengths with those in the experiment

of Burkhalter and Koschmieder [7]. From the figure, a consistent trend was evident: the axial wavelength (λ) of Taylor vortices decreased rapidly with Taylor number when the Taylor number ratio (Ta/Ta_c) was larger than four. There was a *plateau* (named by Koschmieder [7]) when Ta/Ta_c values were between two to four. λ *then* kept increasing up with the decrease of Ta. <mark>Considering the uncertainty in the experimental data, clearly, the CFD solver employed in the present study is capable of matching the number and spacings of Taylor vortices over a range of experimental conditions.</mark>
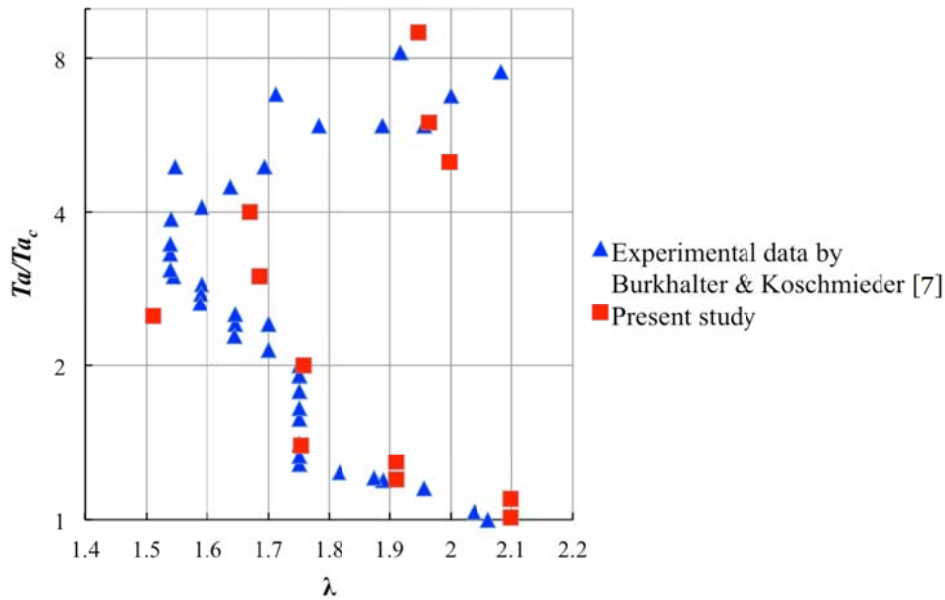

Fig.3. The axial wavelength (λ) of Taylor vortices at various Taylor numbers (Ta/Ta_c). (Experimental data shown was obtained by [7])
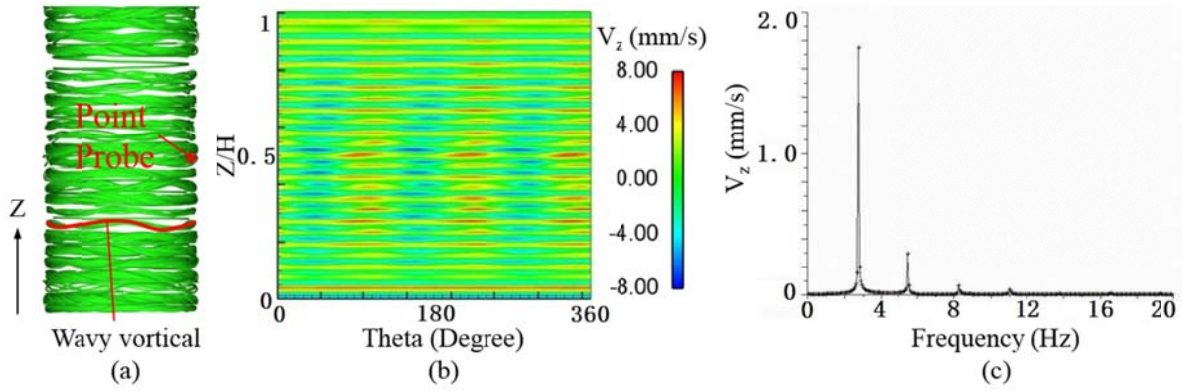
Fig. 4.   (a) Illustrations of instantaneous wavy vortical structures, (b) Mid-gap surface colored by z direction velocity, (c) FFT of z direction velocity obtained from a point probe.

Test Case 2: Wavy Taylor-Couette Flow [8]

In the second part of the validation study, the experimental results of Kingt [8] were used to verify the capability of the CFD solver in predicting the wavy Taylor-Couette flow. All boundary conditions for the CFD simulations were taken from the experiment by Kingt [8]. Three different cases with varying radius ratios were simulated and all the cases shared the same geometry parameters and boundary conditions as ones employed in the real experiment. The aspect ratio was maintained to a value of 30 for all the cases and the rotating speed was set to be 11 times the real critical value. Both ends of the annulus gap were set to be no-slip wall. The fluid material was water with a viscosity of 0.001003 kg/m-s and a density of 998 kg/m^3. For the case with the radius ratio of 0.868, an illustration of the wavy vortical flow structures present in the shaft gap is shown in Fig. 4(a). Fig. 4(b) presents an expanded view of axial Z-velocity (Vz) contour along the mid-gap surface. Additionally, the azimuthal wave number (m) can also be directly read out by counting the vortices in the contour plot. During the simulation, a point probe was specified in the middle gap to record the unsteady variation of the Z-velocity. The fundamental frequency of the azimuthal waves

11

(f) was then derived by Fast Fourier Transform of the unsteady signal (FFT), as shown in Fig. 4(c).

The wave speed (s) is defined as,

$$s = \frac{2\pi f}{m\Omega_1}.$$ (3)

The final simulation results are presented in Table 1. Qualitatively, the computed results showed consistently the trend seen in the experiment that the wave speed increases with increasing radius ratios. Quantitatively also, the discrepancies between the three computed cases and the experimental data were within an acceptable range.

Table 1 Wave speed values achieved from simulation and experiment at three different η.

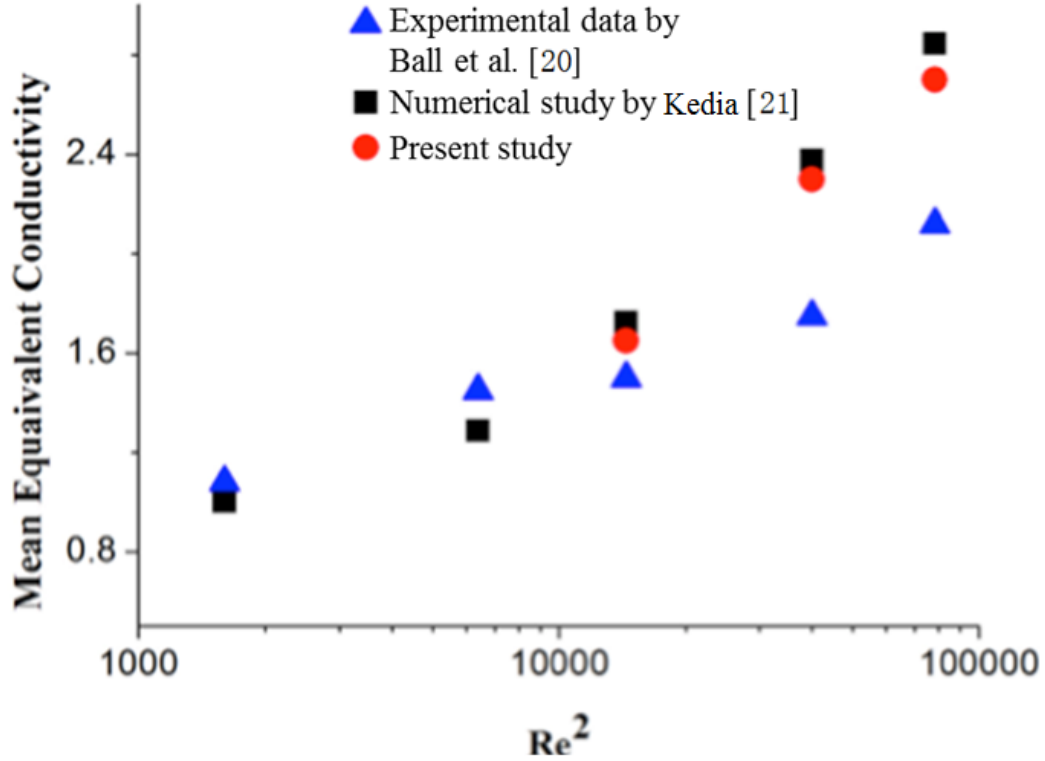| η(R_1/R_2)	Present study	Experimental results
0.868	0.334	0.320±0.005
0.900	0.362	0.360±0.010
0.950	0.458	0.450±0.001

Fig. 5. Comparisons of mean equivalent conductivity between data from [20, 21] and the present study.

Test Case 3 :Heat transfer in Taylor-Couette Flow [20]

In addition to the validation of the solver for flowfield variations, the published data of Ball et al. [20] was used to validate the thermal prediction capability of the solver. Heat transfer phenomena in Taylor-Couette flow with radial temperature gradient were studied in this section of the paper. In order to systematically investigate the effects of both the buoyancy and the centrifugal forces on the flow stability, the local mean equivalent conductivity (k_{eq}) was chosen to be the key parameter for comparison. It was defined as,

$$K_{eq} = -hr\ln(\eta)/k, \tag{4}$$

where h is the average heat transfer coefficient in the inner cylinder surface, k is the thermal conductivity, and r is the radial coordinate.

The computational geometry and the boundary conditions for this study were based on the experimental set up of Ball et al. [20], which were: the inner and outer cylinders were set to be 0.01252 m and 0.02216 m respectively (η=0.565). The height of the annulus gap was 0.5064 m. In order to maintain Grashof number at 100 (the temperature difference between two cylinders was 7.582 K), the inner cylinder was specified to be a no-slip wall with an isothermal surface temperature of 293.000 K, while the outer cylinder was set to have a temperature of 300.582 K. The fluid material was air, with a density of 1.175 kg/m^3, thermal conductivity of 0.0257 w/m-k and kinematic viscosity of 15.11×10−6 m^2/s. In total three different cases with varying rotating speeds (5.008 rad/s, 15.023 rad/s and 35.054 rad/s) were simulated. All the cases were simulated under laminar regime since the maximum corresponding Reynolds number was much less than the critical Reynolds number for η of 0.565.

The computed results is compared with the experimental data of Ball et al. [20] in Fig. 5. As an additional reference, Figure 5 also presents numerical results by Kedia [21] who have conducted CFDl study to simulate the same case by Ball et al. [20]. It is evident from the figure that two simulations are seen to show a consistent trend, however the CFD results show some discrepancies with the experimental data (especially at higher Reynolds number). Kedia [21] suggested that such discrepancy was due to the variation of the axial wave along the cylinders caused by the uncertain thermal conditions of the end walls in the experimental set up.
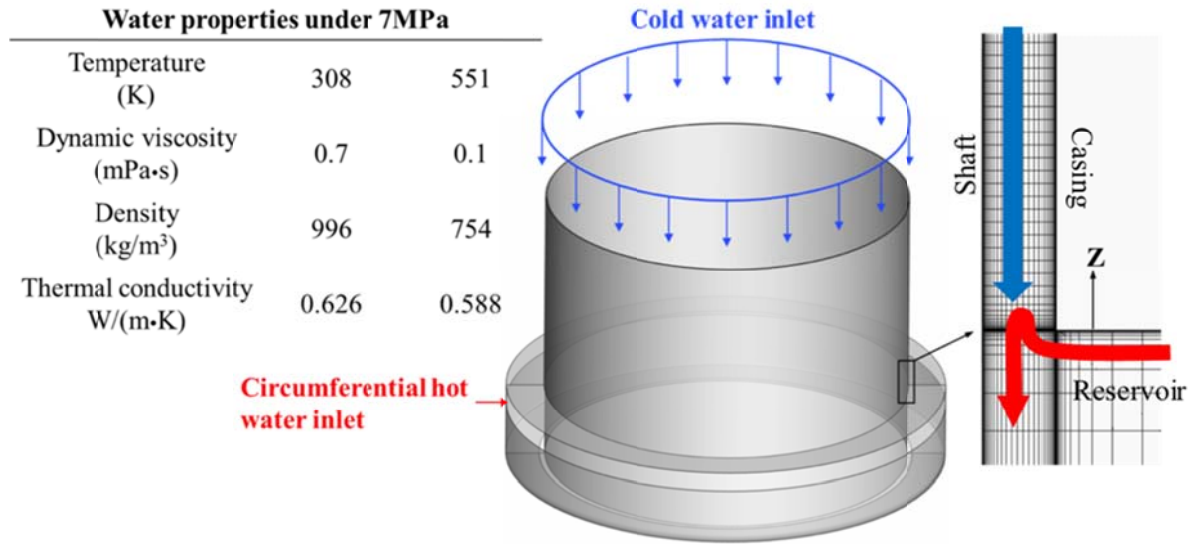
Water properties under 7MPa		
Temperature (K)	308	551
Dynamic viscosity (mPa·s)	0.7	0.1
Density (kg/m³)	996	754
Thermal conductivity W/(m·K)	0.626	0.588

Fig. 6. Computational domain and grids for the present study

COMPUTATIONAL DETAILS FOR THE PLR PUMP APPLICATION

From the validation exercise presented above, it is verified that FLUENT is an appropriate solver to simulate the Taylor-Couette flow in all conditions with or without temperature factor involved. Hence in the next step, a more complicated geometry which is representative of a practical scenario is considered to simulate the flow around a shaft in a PLR pump. Fig. 6 shows the geometrical details and the computational domain used for the PLR pump.

The details of the computational domain used in the PLR pump simulation are listed as follows. To match the conditions in the work of Watanabe et al. [14], the height of the annulus gap was 140 mm, outer and inner radiuses were 97.5 mm and 96.85 mm respectively (η=0.993). The top inlet flow rate was kept to be 0.0691 kg/s and the temperature was set at 308 K. Three different cases were simulated with varying values of the shaft rotating speed, i.e., 146 rad/s, 100 rad/s and 80 rad/s. The circumferential cold

was set to be 10 times of the maximum inlet velocity and it was kept constant for all the cases simulated. The temperature of the fluid from the circumferential inlet was also varied for the three cases, which were 308 K, 450 K and 551 K. Notice that 551 K is the maximum temperature that may appear in the real pump operating condition. No-slip wall boundary condition was set at all the wall boundaries.

The material of the fluid was defined by User Defined Function (*UDF*) file based on the physical properties of the water under 7 MPa. The water properties labeled in Fig. 6 are based on database provided by Cengel and Boles [23] and large variations of viscosity, density, and thermal conductivity of the water exist within the temperature range investigated. Therefore, fully compressible flow option in FLUENT (density-based solver) was used in this simulation.
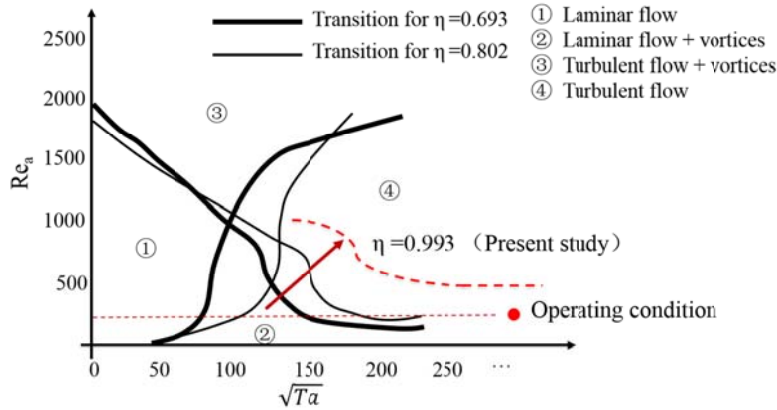

Fig. 7. Validation of laminar flow condition in the present study against flow regimes provided by [25].

As discussed in the previous section, there are many different forms of Taylor-Couette flow instabilities. The flow under the present investigation is within the laminar flow regime. This can be verified by comparisons with two sets of data from the open literature. Firstly, Di Prima and Swinney [24] showed that the critical rotation speed for Taylor vortices is 10 rad/s for the radius ratio values close to 1 (similar to present study). Their experimental data show the flow transition from laminar to turbulence appears at almost 20 times of the critical

Taylor number. A rotating speed of 146 rad/s employed in the present study is inadequate for the transition to occur. Note that it has also been confirmed that the axial flow will further delay the formation of Taylor vortices. This had not been taken into account by Di Prima and Swinney [24], which makes the present laminar assumption more valid. Secondly, Kaye and Elgar [25] summarized typical flow regimes at various axial flow Reynolds and Taylor numbers. The transition lines between the laminar and the turbulent flow regimes for radius ratios of 0.693 and 0.802 are shown in Fig. 7. In the present study, the radius ratio is 0.993. An approximate line (red dashed line in Fig. 7) was extrapolated from these two existing transition lines by Kaye and Elgar [25]. It can be seen that the operating condition for the present study (axial Reynolds number is 217.5 and Taylor number is 9154.4) should be in the laminar flow regime, as shown by the red marker in the figure.

RESULTS AND DISCUSSIONS

The following section describes the influence of the temperature difference between the axial purge and cavity fluids on the flow field in the gap between the rotating shaft and stationary casing.

For a case with uniform temperature of 308 K and inner cylinder rotating speed of 146 rad/s, Fig. 8(a) shows the temporal development of the normalized z direction velocity Vz contours during one period of flow movement at one circumferential plane near the interface region between the upper shaft gap and hot water cavity (the end of the annulus gap). The instantaneous z direction velocity distribution around the circumference in the middle of the gap is shown in Fig. 8(b). Physical locations of the circumferential and mid-gap planes were marked in both figures as vertical dashed lines. Red colors in the contours indicate the upward flow whereas the blue colors represent the downward flow.

17

The purge flow dominates the flow field at the beginning of the period, as shown in the circumferential plane in Fig. 8(a). The region where the cold purge flow penetrates the downstream cavity moved around the circumference by time. As the purge flow moves away, Taylor instabilities start to develop, pairs of counter-rotating vortices are formed in the gap. In the middle part of the transient period, Taylor vortices dominate the dynamics of the flow in the gap. Influenced by the new purge flow approaching this location, the vortices start to stretch and merge (indicated by dashed lines in Fig. 8(a)). During the majority of the transient period, all the vortices in the flow are gradually moving downward (line II) before the purge flow dominates again. Spatial development of such convection process of the vortical structure is demonstrated by the z direction velocity contour along the mid-gap surface shown in Fig. 8(b). From this typical wavy Taylor vortical flow structure, it can be clearly observed that the transient period shown in Fig.4.3(a) is repeated four times (line I) during one revolution of the shaft (azimuthal wave numbers m=4).
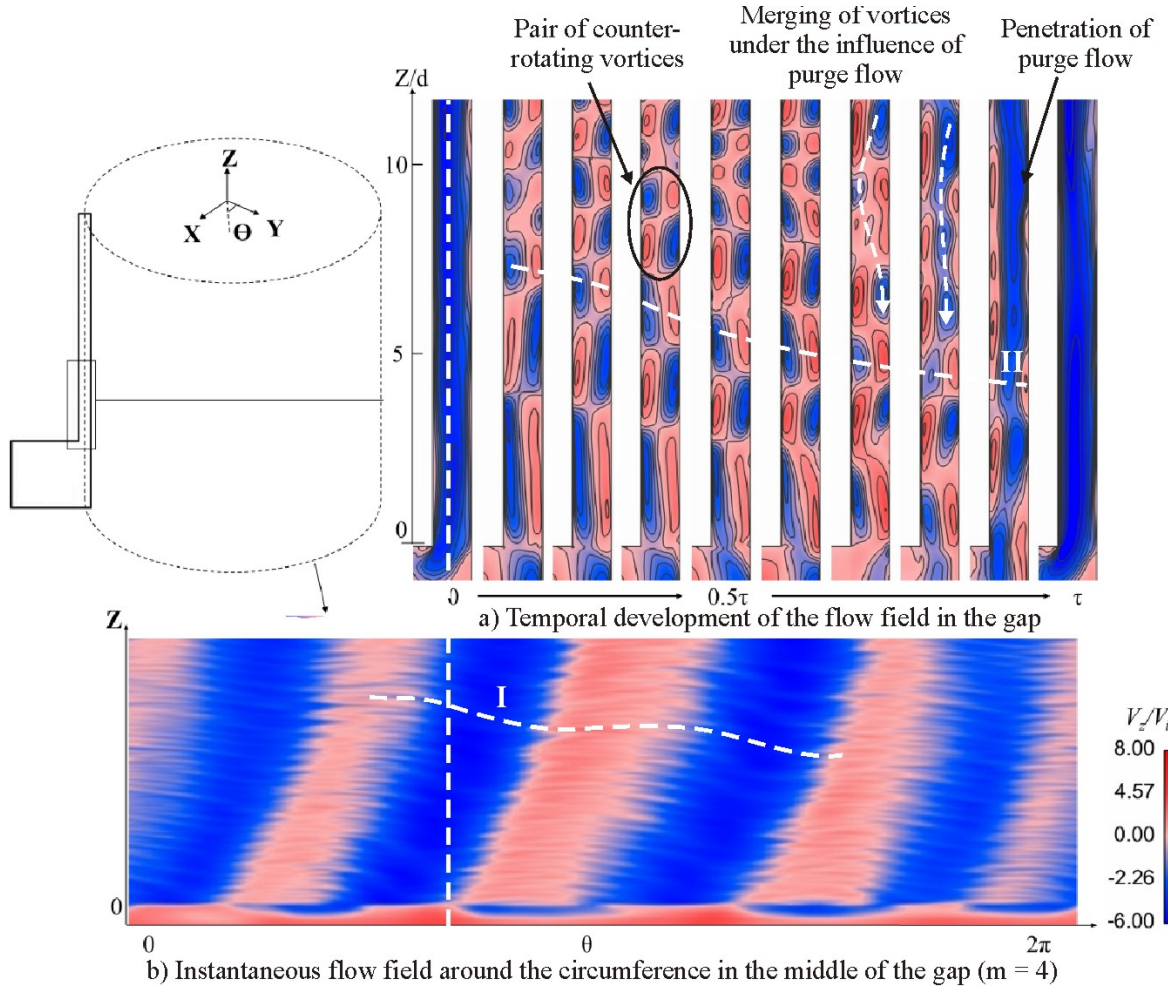
Fig. 8. Normalized z direction velocity *Vz* contours during one period of flow movement at one circumferential plane and instantaneous z direction velocity *Vz* distribution around the circumference in the middle of the gap. Case with no temperature difference.

Flow structures for cases with temperature difference between the two inlets are presented as below. As a good comparison with Fig. 8, Fig. 9 shows similar distributions of normalized z direction velocity near the end of the annuls gap, again driven by the purge flow dynamics, but with large temperature difference (cold inlet temperature of 318 K and hot inlet temperature of 551 K). Figure 9 shows that as the purge flow moves away, the cavity fluid penetrates upwards into the gap causing the stretching of the local vortical flow structures. It can be also seen that the upwards moving cavity fluid maintains its position in the vicinity of inner rotating shaft surface (indicated by red color contours). This simulation

visualizes the direct reason why the shaft and casing cover would suffer temperature fluctuation. Such result also well predicts the place having the largest temperature fluctuation, where is close to the interface region of annulus gap and hot water cavity. Additionally, there are clearly three periodic waves appearing in the mid-gap surface, one less than the wave number shown in Fig. 8.
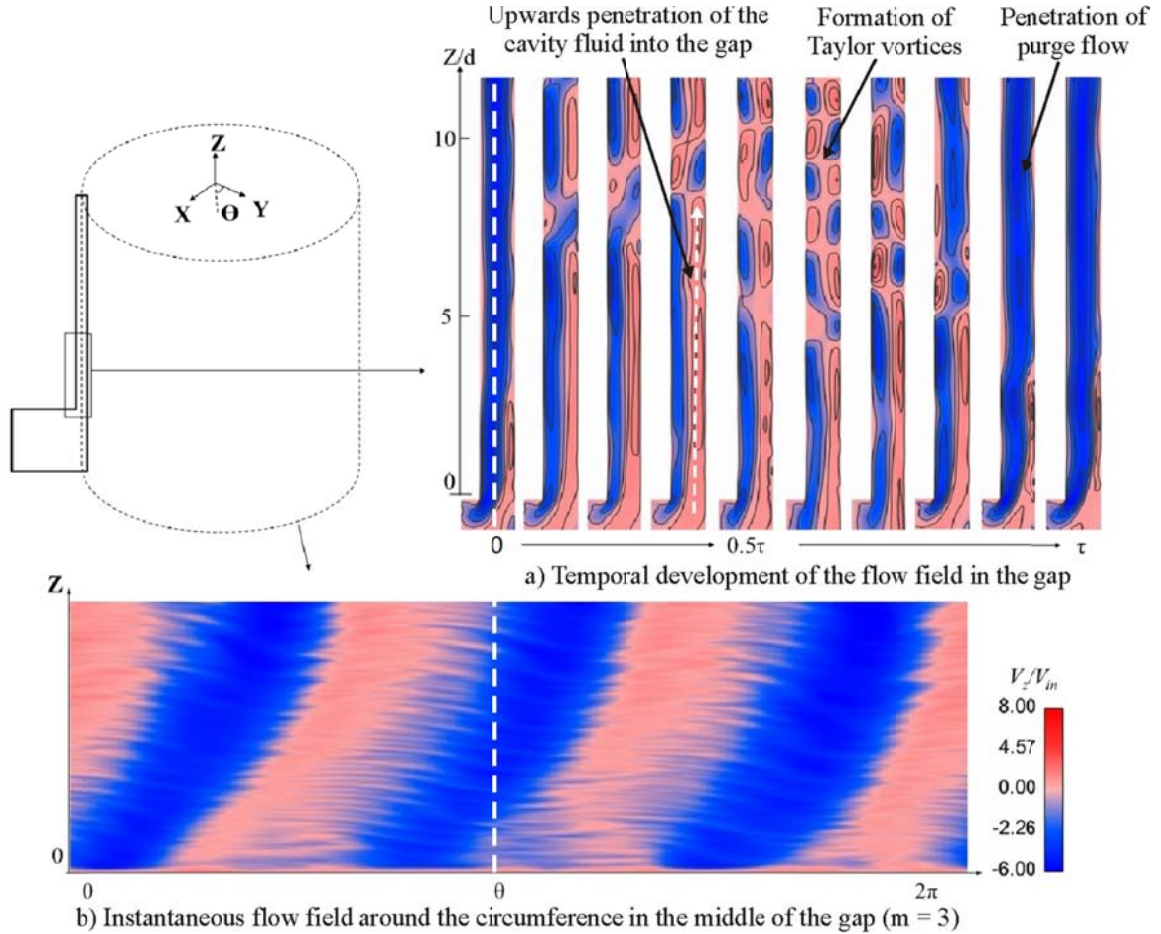

a) Temporal development of the flow field in the gap

b) Instantaneous flow field around the circumference in the middle of the gap (m = 3)

Fig. 9. Normalized z direction velocity *Vz* contours during one period of flow movement at one circumferential location and instantaneous z direction velocity Vz distribution around the circumference in the middle of the gap. Case with temperature difference of 243 K.

Figure 10 presents the temporal development of vortical structure near the interface region between the annulus gap and lower hot water cavity for cases without and with temperature differences (cold inlet temperature of 308 K and hot inlet temperature of 551 K). The vorticity color field were obtained by using ten time steps during one period of the

transient process. ==Two dimensional streamlines generated by projecting the tangential velocity vector on the plane were also added to the contour plot to illustrate the stretching of Taylor vortices in the flow.==

For both of the cases, Taylor vortices form in the middle part of one period and seem to be disappearing at the beginning and ending time. Further in aspect of movement, it can be seen that, for both cases, the axial flow shows with a sinuous nature, passing through the space between adjacent vortices. And the strength of the axial flow periodically changes. It is because that as long as the bottom vortex was pushed out of the annulus gap or forced to be deformed (in case with temperature difference), the axial flow will rush out until new Taylor vortices form again. The difference in flow structure is evident for two cases. Besides the content mentioned in the last section, the vortices in case without temperature difference has more uniform structure and the size of the vortex at the bottom decreased until it was completely pushed out of the annulus gap. For the case with temperature difference, the number of the vortices developed in the gap region close to the interface with the downstream cavity is reduced and the bottom vortex is greatly stretched. That vortex is pushed by the downward axial flow. Therefore, the size of it should be decreasing theoretically. However, the contacting vortex sometimes merges into it and elongation will happen consequently. Clearly, in addition to the stretching of the local vortical flow structure, ==all the fluids near the end of the annulus gap are moving upward attaching the surface of inner rotating shaft (indicated by red color contours).==
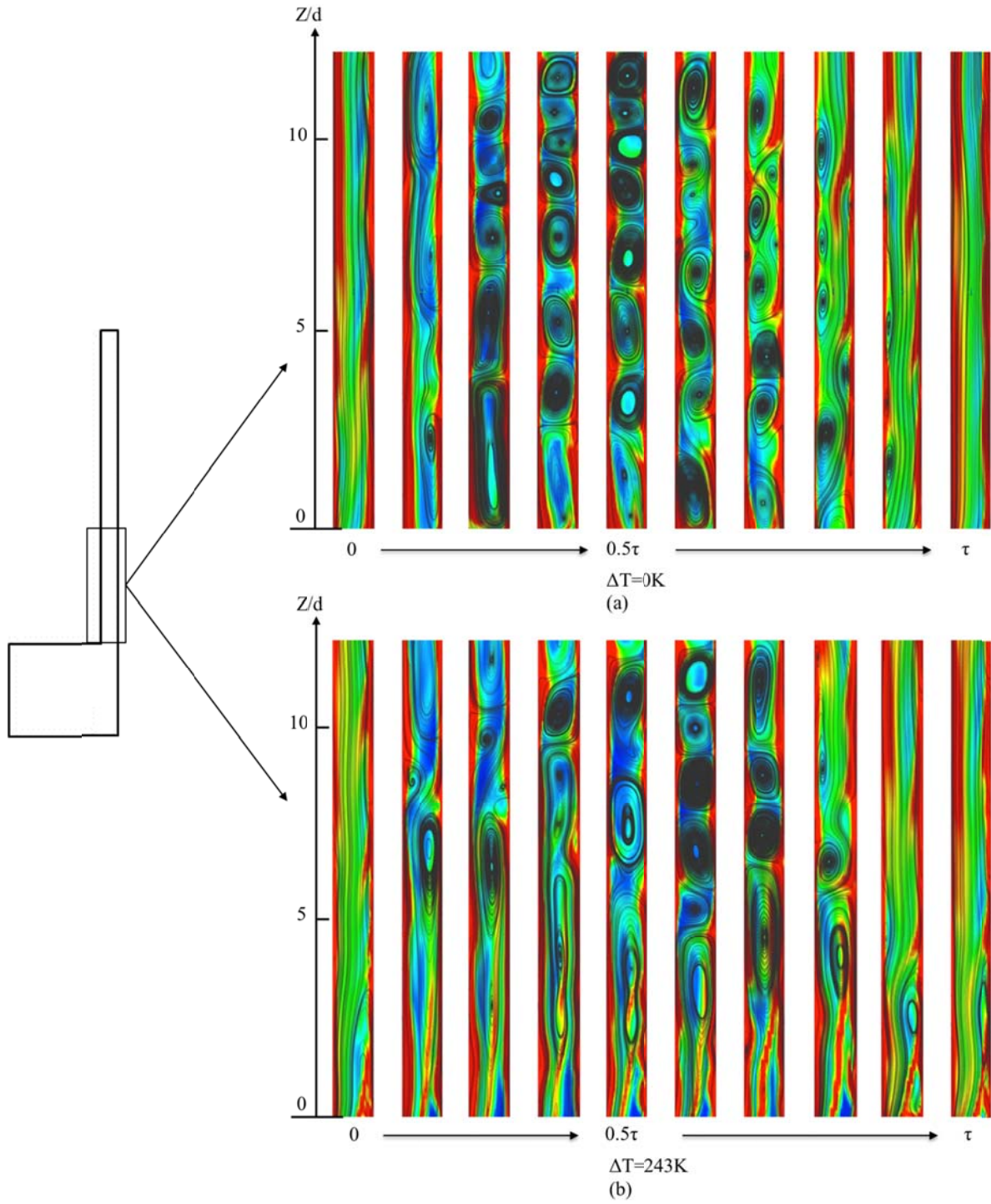
Fig. 10. Instantaneous vorticity contours and streamlines at ten different time instances during one period, for cases with and without temperature differences.
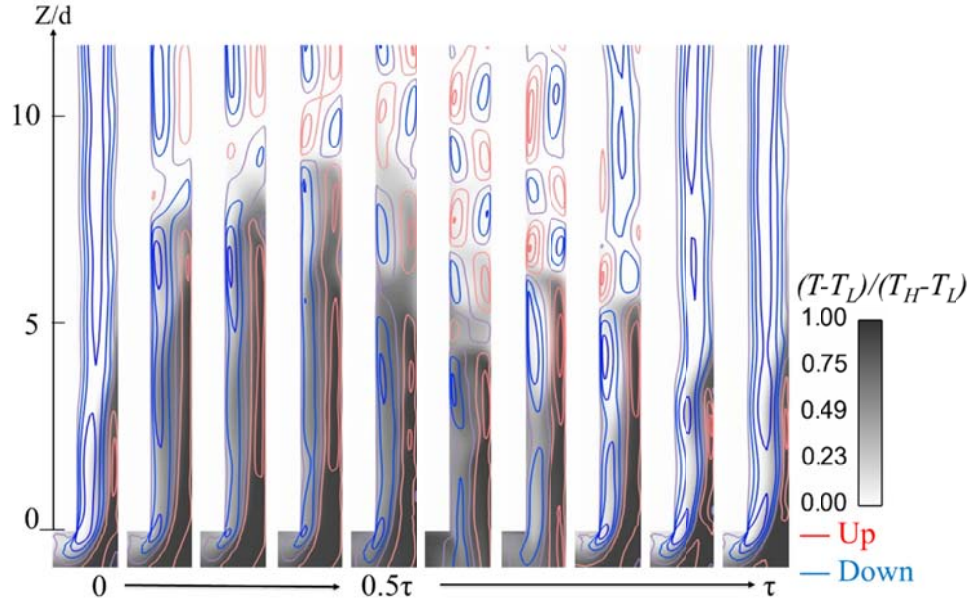
Fig. 11. Temporal development of the Normalized temperature distribution with lines indicating the flow structure in the gap during one period at one circumferential location.

Figure 11 illustrates the variation of temperature distribution within the gap flow during one period of the unsteady process, with the cold inlet temperature of 308 K and hot cavity temperature of 551 K. Non-dimensional temperature is colored by grey scale. Structure of Taylor vortices is also shown by additional lines with red and blue colors. Consistent with the color shown in Fig. 8 and Fig. 9, the red color indicates upwards flow direction, while the blue color represents downwards direction. Clearly, it is the hot water which moves upwards and stay concentrated to the shaft near the transition region.

The variation in temperature in the shaft gap causes the density variation within the gap consequently. The buoyancy force due the density gradient plays an important role in modifying shapes (stretching) of the Taylor vortices flow structure. It is expected that the hot water is pushed upwards by the buoyancy effect and brings additional resistance to the cold fluids coming down along the gap. So far, the reason of why larger temperature difference will decrease the fluctuation frequency of the vortices has become clear. In detail, this hot flow can be regarded as an obstacle to prevent Taylor vortices from coming downward and

23

oscillating with high frequency. The larger temperature difference is, the stronger such obstacle will be. The movement of the vortices are constrained consequently.

Figure 12 gives more details of the flow structure between the shaft and the casing. The streamlines in Fig. 12 oscillate azimuthally, which also indicates that hot fluids are raised up periodically from the cavity.
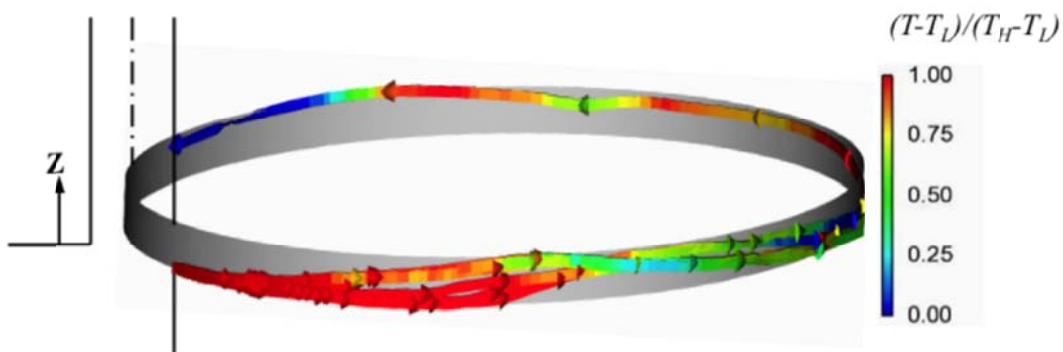

Fig. 12. Streamlines near the interface region.

Figure 13 presents the instantaneous velocity vectors for the fluid near the interface region with the existence of temperature difference during one transient period. The background is colored by normalized temperature. For all four vector fields taken, the large cavity flow structure remains similar. With a large counter-rotating vortex in the far field (detail A), a clock-wise vortex (detail B) always occur in the near shaft region and keeps pumping up the hot fluid from the cavity to the gap, even with and without the purge flow approaching the same circumferential location. The hot fluid is oscillating near the shaft at a certain distance above the cavity (detail C) (causing the shaft thermal fatigue at this axial location).

There are two possible reasons for the phenomenon that fluid in the cavity comes upward attaching the shaft surface. The first reason is that the relatively low density fluid (high temperature) tends to stay closer to the near shaft region due to the centrifugal force.

The other one is that the pressure near the shaft is lower than that near casing cover and in the cavity, it is because the fluid near the shaft is enforced with higher moving velocity.
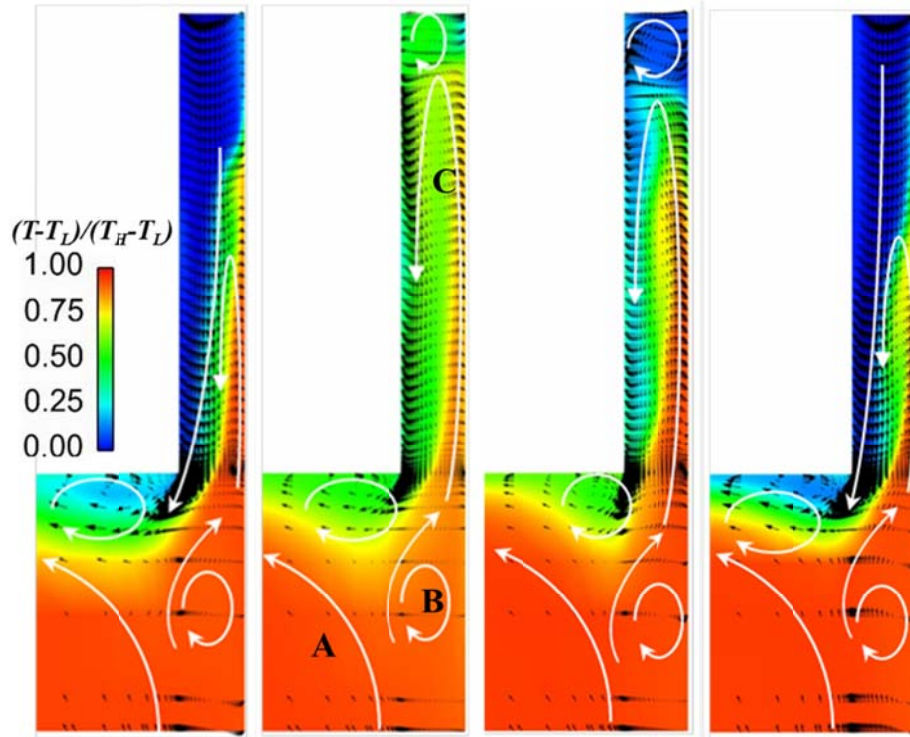

Fig. 13. Instantaneous velocity vector fields taken during one transient period near the interface close to the downstream cavity.

With the increasing temperature difference between the cold inlet flow and hot water cavity, the axial location of the maximum temperature fluctuation, i.e., the maximum radial penetration of the hot fluid, moves up along the shaft wall, as shown in Fig. 14(a). The hot fluids are pushed much higher near the shaft surface due to relatively larger buoyancy force. In the experimental study by Watanabe et al. [14] with the same geometry and boundary conditions, a shaft location Z/d value of 7.84 was reported as the location where the maximum temperature fluctuation occurred. This agrees well with the present case under temperature difference of 243 K shown in Fig. 14(b).
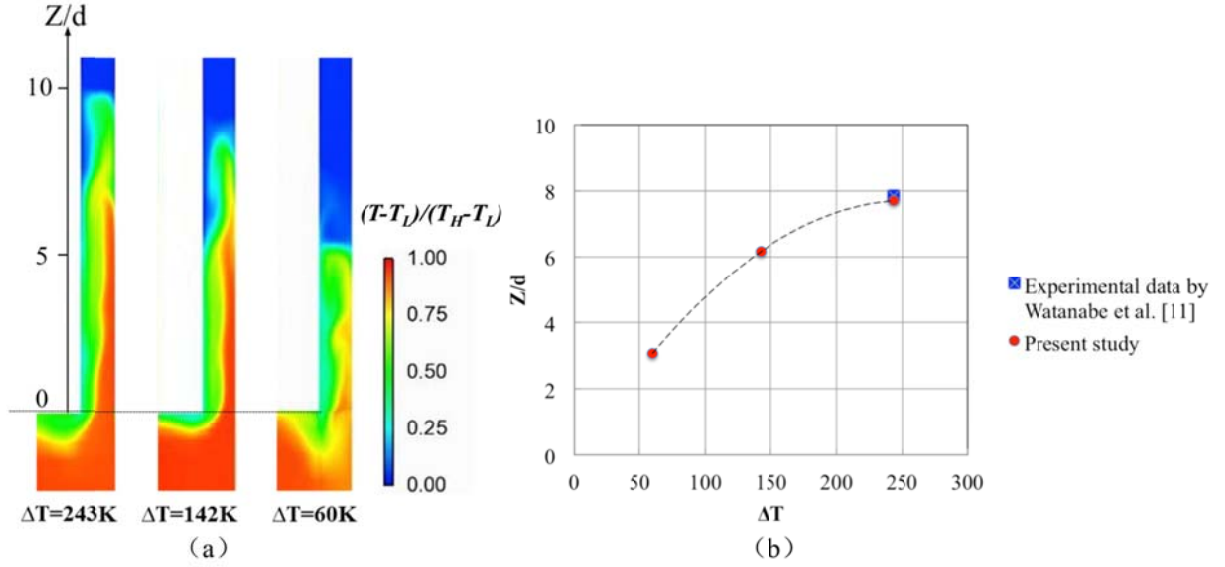
Fig. 14.   (a) Non-dimensional temperature contours when the upwards hot fluid reach its maximum height, and (b) locations where the maximum temperature fluctuation occurs at cases with different temperature difference.

Table 2 Wave number and frequency under different temperature conditions.

T_L(K)	T_H(K)	Azimuthal frequency f (Hz)	Azimuthal wave number m	Wave speed s
308	551	20.5	3	0.294
308	450	25.5	4	0.274
308	308	26.0	4	0.280
450	450	26	4	0.278
551	551	21	3	0.298

Table 2 summarizes the azimuthal wave number (*m*), fundamental frequency of the azimuthal waves (*f*) and wave speed (*s*) for cases with varying water temperature magnitudes. With uniform temperature in the flow field, both the frequency and azimuthal wave number reduce at higher temperature, while the wave speeds of the azimuthal waves stay nearly constant. A similar trend was observed by [8], who studied the wavy Taylor

vortices without the existence of axial flow. Such trend is mainly due to the reduction in viscosity of the fluid. Table 2 also indicates that lower azimuthal frequency and smaller wave number are associated with higher temperature differences.

For the case with ΔT=243 K, the instantaneous normalized temperature at one location of the shaft wall surface (near the interface region) is plotted in both time and frequency domains, as shown in Fig. 15(a) and (b), respectively. Figure 15 also presents the corresponding z velocity fluctuations of the near wall fluid at the same vertical location (dashed-line). Apparently, the velocity and temperature fluctuations synchronize with each other, which reveals an important fact that the thermal fatigue in practice is mainly driven by the oscillation of the local unsteady flow field.
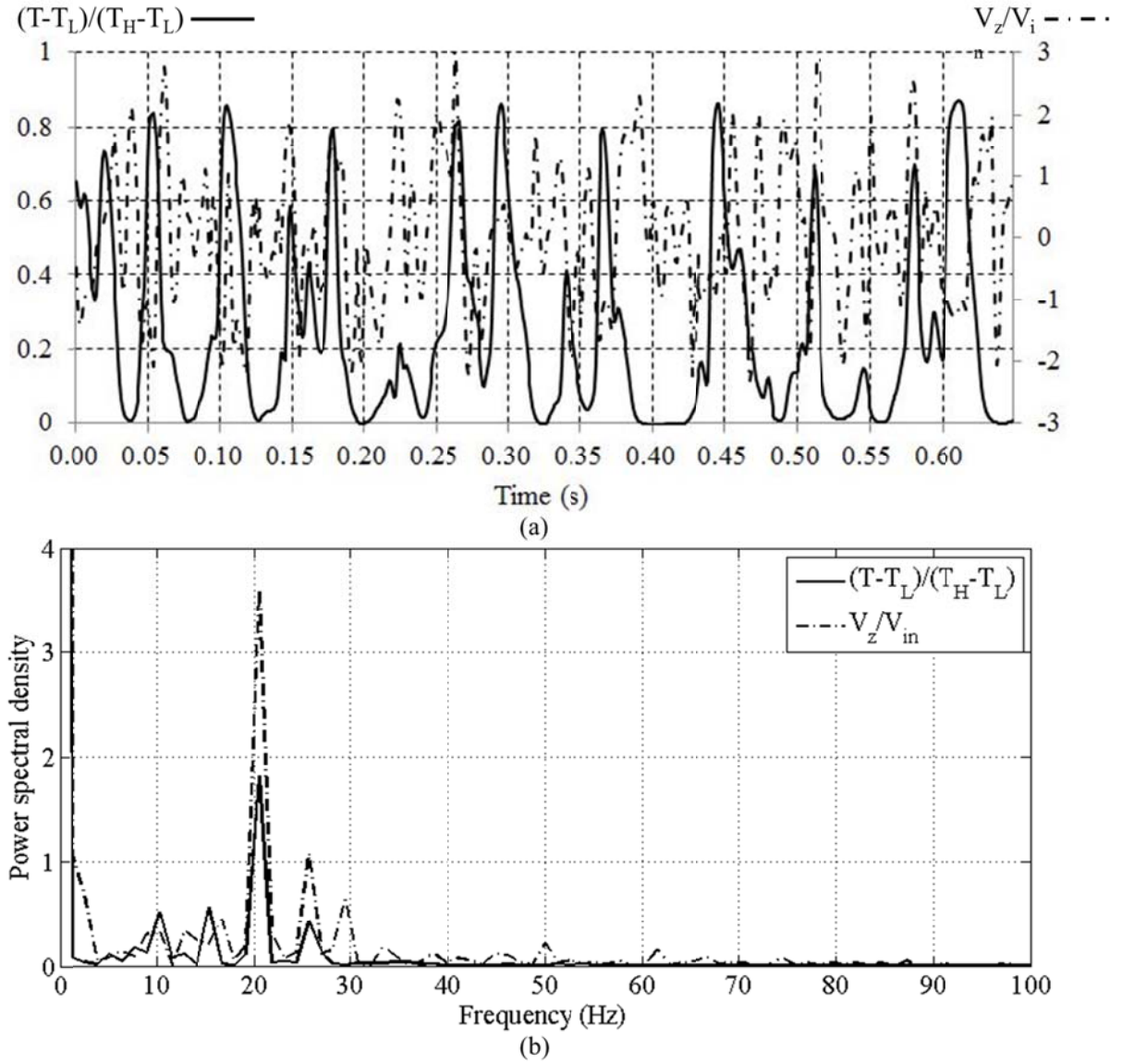
Fig. 15. Fluctuations of normalized temperature and z velocity at one shaft location near the interface region at (a) time domain, and (b) frequency domain (PSD). (ΔT=243 K)

Note that the axial thermal conduction along the shaft and casing was neglected in the present study. Therefore uncertainties exist while comparisons to the real operating condition are to be made.

CONCLUSION

This paper presents a numerical study on the effect of temperature gradient on the Taylor-Couette flow instabilities in the PLR pump of the nuclear power plants. The capability of the computational solver employed was extensively validated against published experimental data in the open literature.

For both cases with and without the temperature gradient, the mechanism of Taylor instability formation is similar, and the azimuthal wave speed of the wavy Taylor vortices stays nearly constant. With the existence of larger temperature difference, the local Taylor vortical structure near the interface between the annulus gap and lower cavity stretches greatly along the gap. The hot fluid from the lower cavity penetrates upwards into the gap, and mostly maintains its position in the vicinity of inner rotating shaft surface (driven by the centrifugal force). Higher temperature difference and rotating speed induce lower fluctuating frequency and smaller circumferential wave number of Taylor vortices. However, the azimuthal wave speed remains unchanged with all the cases tested.

The predicted axial location of the maximum temperature fluctuation on the shaft is in a good agreement with the experimental data. The temperature fluctuation is strongly synchronized with the unsteady flow movement.

It is in the hope that the new physical understandings presented in this paper would help the future PLR pump shaft-casing design optimization to ease the thermal fatigue problem in practice.

NOMENCLATURE

H	Annulus gap height (m)
h	Average heat transfer coefficient in the inner cylinder surface(W/(m^{2}K))
λ	Axial wavelength
s	Azimuthal wave speed
Ta_c	Critical Taylor number
f	Fundamental frequency of the azimuthal waves (Hz)
d	Gap width=R_2-R_1(m)
Z	Height from the end of the annulus gap (m)
T_H	Highest temperature (K)
V_{in}	Inlet velocity (m/s)
v	Kinematic viscosity (m^2/s)
k_{eq}	Local mean equivalent conductivity
T_L	Lowest temperature (K)
m	Number of azimuthal waves
τ	Period time (s)
r	Radial coordinate (m)
R_1	Radius of inner cylinder (m)
R_2	Radius of outer cylinder (m)
η	Radius ratio=R_1/R_2
Ω_1	Rotating speed of the inner cylinder (rad/s)
Ω_2	Rotating speed of the outer cylinder (rad/s)
Re	Reynolds number
Ta	Taylor number which is defined as $\frac{\Omega d R_1}{v}$
k	Thermal conductivity
V_z	Z-direction velocity (m/s)

REFERENCES

[1] Koschmieder, E. L., 1993, "Bénard cells and Taylor vortices," Cambridge University Press.

[2] Taylor, G. I., 1923, "Stability of a viscous liquid contained between two rotating cylinders," Philosophical Transactions of the Royal Society of London, Series A, Containing Papers of a Mathematical or Physical Character, 223, 289-343.

[3] Andereck, C. D., Liu, S. S., & Swinney, H. L., 1986, "Flow regimes in a circular Couette system with independently rotating cylinders," Journal of Fluid Mechanics, 164(3), 155-183.

[4] Sparrow, E. M., Munro, W. D., & Jonsson, V. K., 1964, "Instability of the flow between rotating cylinders: the wide gap problem," Journal of Fluid Mechanics, 20(1), 35-46.

[5] Roberts, P.H., 1965, "The solution of the characteristic value problem," Proceedings of the Royal Society of London Series A(283), 550-556

[6] Cognet, G., 1984, "Les étapes vers la turbulence dans l'écoulement de Couette-Taylor entre cylindres coaxiaux," Journal de mécanique théorique et appliquée, 7-44.

[7] Burkhalter, J. E. and Koschmieder, E. L., 1974, "Steady supercritical Taylor vortices after sudden starts," Physics of Fluids, 17.

[8] Kingt, G. P., 1984, "Wave speeds in wavy Taylor-vortex flow," Journal of Fluid Mechanics,141.

[9] Wereley, S. T. and Lueptow, R. M., 1999, "Velocity field for Taylor–Couette flow with an axial flow," Physics of Fluids, 11.

[10] Becker, K. M. and Kaye, J., 1962, "The influence of a radial temperature gradient on the instability of fluid flow in an annulus with an inner rotating cylinder," Journal of Heat Transfer (US), 84.

[11] Martin, B. W., and Hasoon, M. A., 1976, "The stability of viscous axial flow in the entry region of an annulus with a rotating inner cylinder," Journal of Mechanical Engineering Science, 18(5), 221-228.

[12] Narabayashi, T., Miyano, H., Komita, H., Iikura, T., Shiina, K., Kato, H., ... & Takahashi, Y., 1993, "Study on temperature fluctuation mechanisms in an annulus gap between PLR pump shaft and casing cover," In the 2nd ASME-JSME Nuclear Engineering Joint Conference, San Francisco, CA, USA, 207-213.

[13] Kato, H., Kanno, H., Hosokawa, M., Watanabe, A., Shitara, C., Ashizawa, K., ... & Iikura, T., 1992, "Development of advanced nuclear primary loop recirculating pump (PLR pump) for BWR plant considering thermal fatigue problem," In Winter Annual Meeting of the American Society of Mechanical Engineers, Anaheim, CA, 157-162.

[14] Watanabe, A., Takahashi, Y., Igi, T., Miyano, H., Narabayashi, T., Ikura, T., Sagawa, W., Hayashi, m., Endo, A., Kato, H., Kanno, H., Hosokawa, M.., 1993, "The study of thermal fatigue problem on reactor recirculation pump of BWR plant," Elsevier Sci. Pr. B.V., 383-388.

[15] Gazley, C., 1958, "Heat transfer characteristics of the rotational and axial flow between concentric cylinders," Journal of heat transfer, 80(1), 79-90.

[16] Tachibana, F., & Fukui, S., 1964, "Convective heat transfer of the rotational and axial flow between two concentric cylinders," Bulletin of JSME, 7(26), 385-391.

[17] Aoki, H., Nohira, H., and Arai, H., 1967, "Convective heat transfer in an annulus with an inner rotating cylinder," Bulletin of JSME, 10(39), 523-532.

[18] Fenot, M., Bertin, Y., Dorignac, E., & Lalizel, G., 2011, "A review of heat transfer between concentric rotating cylinders with or without axial flow," International journal of thermal sciences, 50(7), 1138-1155.

[19] Liu, D., Kang, I. S., Cha, J. E., & Kim, H. B., 2011, "Experimental study on radial temperature gradient effect of a Taylor–Couette flow with axial wall slits," Experimental Thermal and Fluid Science, 35(7), 1282-1292.

[20] Ball, K. S., Farouk, B., & Dixit, V. C., 1989, "An experimental study of heat transfer in a vertical annulus with a rotating inner cylinder," International Journal of Heat and Mass Transfer, 32(8), 1517-1527.

[21] Kedia, R., 1997, "An investigation of velocity and temperature fields in Taylor-Couette flows."

[22] Shiina, K., Nakamura, S., Mizushina, Y., Yanagida, T., Endo, A., Takehara, H., ... & Kato, H., 1996, "Heat transfer characteristics of fluid flow in an annulus with an inner rotating cylinder having a labyrinth structure," Heat Transfer‐Japanese Research, 25(2), 103-119.

[23] Cengel, Y. A., & Boles, M. A., 2011, Thermodynamics: an engineering approach (Vol. 5), New York: McGraw-Hill.

[24] Di Prima, R. C., and Swinney, H. L., 1985, "Instabilities and transition in flow between concentric rotating cylinders," In Hydrodynamic instabilities and the transition to turbulence, Springer Berlin Heidelberg, 139-180.

[25] Kaye, J. and Elgar, E. C., 1957, "Modes of adiabatic and diabatic fluid flow in an annulus with an inner rotating cylinder," MIT Research Laboratory of Heat Transfer in Electronics.